Structure and Optical Properties of Ferroelectric $PbZr_{0.40}Ti_{0.60}O_3$ Films Grown on $LaNiO_3$−Coated Platinized Silicon Determined by Infrared Spectroscopic Ellipsometry

Z. G. Hu,*,† Y. W. Li,† M. Zhu,‡ Z. Q. Zhu,† and J. H. Chu†,§

Key Laboratory for Polar Materials and Devices, East China Normal University, Shanghai 200241, People's Republic of China, Department of Physics, Shanghai Jiao Tong University, Shanghai 200240, People's Republic of China, and National Laboratory for Infrared Physics, Shanghai Institute of Technical Physics, Chinese Academy of Sciences, Shanghai 200083, People's Republic of China

Received: February 22, 2008; Revised Manuscript Received: April 18, 2008

The $PbZr_{0.40}Ti_{0.60}O_3$ (PZT)/$LaNiO_3$ (LNO) multilayer films with different associated thickness have been deposited on Pt/Ti/SiO_2/Si substrates by a modified sol−gel technique. X-ray diffraction analysis shows that the PZT and LNO films are polycrystalline with the (100)-preferential orientation and perovskite phase. The optical properties of PZT films have been investigated using infrared spectroscopic ellipsometry (IRSE) in the photon frequency range of 800−4000 cm^{-1} (2.5−12.5 μm). By fitting the measured ellipsometric parameters with a four-phase layered model (air/PZT/LNO/Pt) and a derived classical dispersion relation, the optical function and thickness of the films have been uniquely extracted. The refractive index of the PZT films increases and the extinction coefficient decreases with increasing grain size in the mid-infrared region. Correspondingly, infrared absorption coefficient of the films linearly increases with increasing thickness. It can be concluded that the discrepancy of infrared optical properties is mainly ascribed to the crystalline quality, the grain size effect, and the influence from the interface layer. The present results can be crucial for future application of ferroelectric PZT-based infrared optoelectronic devices.

I. Introduction

Much effort has been made on the studies of ferroelectric films with regard to their applications in integrated circuit memories, optical waveguides, electro-optic switches, and pyroelectric imaging sensors.[1–9] The pyroelectric properties of ferroelectric materials in the detection of IR radiation are well-known from single detector and array.[10,11] Recently, uncooled infrared focal plane arrays (IRFPA) based on monolithic ferroelectric film have attracted more attention for the sake of improved performances.[12] Thin film ferroelectric infrared detectors and focal plane arrays, which can be deposited directly on silicon readout integrated circuits, are expected to yield better sensitivity and faster response than the equivalent ceramic and bulk single crystal.[12–16] Among these perovskite ferroelectric materials, $PbZr_{1-x}Ti_xO_3$ (PZT) and doped-PZT films are the most promising compounds for the pyroelectric infrared imaging sensors, which have been successfully applied in manufacturing monolithic pyroelectric film IRFPA.[17] It suggests that some further investigations on the potential materials are necessary to clarify the physical properties, which can provide the theoretical and experimental supports for infrared optoelectronic devices.

Optical and electrical properties of films strongly depend on substrate materials, growth parameters, and deposition methods, which can directly affect the material crystalline quality.[18] Many fabrication techniques are currently applied to prepare these ferroelectric films and lattice-matched conductive oxide electrodes. Among them, sol−gel technique is a well-accepted method due to some evident advantages such as composition control and uniformity, large-area deposition, low cost, and a fast fabrication process.[19,20] Optical and electronic properties are important for design, estimation, and optimization of optoelectronic devices.[21] As we know, dielectric function can be directly related to the electronic band structure of the material. Although there are some reports on optical properties of $PbZr_{1-x}Ti_xO_3$ films on platinized silicon substrates using spectroscopic ellipsometry,[2,22] infrared optical properties of $PbZr_{1-x}Ti_xO_3$ films on conductive oxide bottom electrodes are still required for further studies to elucidate the distinguishing physical behavior. The influence of film thickness on the photon response for optoelectronic devices was found to be significant. This effect must be taken into account in order to assess the practical usefulness of film materials in device applications.[23,24] Similar to $Ba_{1-x}Sr_xTiO_3$ films,[25,26] it can be expected that the film thickness, crystal structure and orientation, grain size distribution, packing density, and morphology of films can strongly affect the optical properties of $PbZr_{1-x}Ti_xO_3$ films. Unfortunately, most studies of film thickness and structure effects in ferroelectric $PbZr_{1-x}Ti_xO_3$ films have been mainly focused on the electrical and ferroelectric properties.[27] To the best of our knowledge, there are no reports on infrared optical properties of $PbZr_{1-x}Ti_xO_3$ films with varied thickness and crystalline structure.

It is well-known that platinum (Pt) electrodes often result in the formation of hillocks and ferroelectric films on Pt electrodes, which exhibit significant fatigue after long bipolar-switching pulses.[28] Fortunately, it has been confirmed that metal-oxide $LaNiO_3$ electrodes can be used to solve these problems. As for the electrodes in ferroelectric film devices, the highly conducting perovskite metallic oxide $LaNiO_3$ films match well with ferroelectric $PbZr_{1-x}Ti_xO_3$ films. The $LaNiO_3$ material, which plays the roles of both electrode and thermal absorption layer, has a relatively large absorption coefficient and shows a more

* Corresponding author. E-mail: zghu@ee.ecnu.edu.cn.
† East China Normal University.
‡ Shanghai Jiao Tong University.
§ Chinese Academy of Sciences.

10.1021/jp801566b CCC: $40.75
Published on Web 06/10/2008

promising application in infrared detectors. Compared with the film on platinized silicon, it is difficult to extract the optical properties of $PbZr_{1-x}Ti_xO_3$ layers on $LaNiO_3$ electrodes from traditional transmittance and reflectance measurements due to the multilayer depth profile. This is also because there are similar optical constants between the bottom electrodes and Pt, which can result in a large correlation coefficient among the fitting parameters.[29,30] Spectroscopic ellipsometry (SE), which is sensitive to ultrathin films and surfaces, is a nondestructive and powerful technique to investigate the optical characteristics of materials.[31,32] In particular, it is very useful to measure the thickness and dielectric function of a multilayer system simultaneously without the Kramers-Krönig transformation (KKT).[32,33] It should be noted that the above drawback can be readily overcome by the variable-angle SE measurement near the Brewster angle of $LaNiO_3$ and/or Pt.[29,33,34]

In this paper, the comprehensive optical properties of $PbZr_{0.40}Ti_{0.60}O_3$ (PZT)/$LaNiO_3$ (LNO) multilayer films with different thickness have been investigated by infrared spectroscopic ellipsometry (IRSE). The objective is to obtain the relationship among mid-infrared optical functions, ferroelctric and bottom electrode film thickness, and crystalline structure of the PZT/LNO heterostructures.

II. Experimental Details

Fabrication of the $LaNiO_3$ Films. The LNO films on Pt/Ti/SiO_2/Si substrates were prepared by a modified sol−gel technique. Analytically pure lanthaum nitrate [$La(NO_3)_3$] (Shanghai Chemical Reagent Co. Ltd.) and nickel acetate [$Ni(CH_3COO)_2{\bullet}4H_2O$] (Shanghai Jiangpu Chemical Reagent Co. Ltd.) were used as the starting materials. Nickel acetate and equimolar amounts of lanthanum nitrate were dissolved in acetic acid and distilled water, respectively. Then, the two solutions were mixed together with constant stirring. Note that the derived system was turbid due to some precipitates. After adding the distilled water with a volume acetic/H_2O ratio of 6:1, the solution system became transparent with the green color. In order to avoid cracking during the heating process, formamide was also added to the solution with a volume H_2O/$HCONH_2$ ratio of 5:1. Finally, the concentration of the precursor solution was adjusted to 0.3 M by adding or distilling some acetic and water.[35] The LNO films were deposited by spin coating at the speed of 4000 rpm for 30 s. Each layer of the films was dried at 160 °C for 5 min, then pyrolyzed at 400 °C for 6 min to remove residual organic compounds, following annealing at 650 °C for 3 min in air by a rapid thermal annealing (RTA) procedure. The thermal treating process for the samples was carried out in an RTA furnace. The heating chamber is composed of two banks of halogen lamps placed above and below a quartz box. Note that the deposition and annealing-treatment procedures were then repeated one, four, and eight times (labeled as A, B, and C) to obtain the different film thicknesses, respectively. The detailed preparation of the films was given in refs 29 and 35. Note that the labels A, B, and C are only corresponding to different film thickness for the LNO layer in order to distinguish three samples. For example, sample A is assigned to the thinner LNO film (i.e., single layer). The following discussions here are based on the uniform sample labels.

Growth of the PZT Films. The PZT films can be obtained using the similar process to the above LNO layers. $PbZr_{0.4}Ti_{0.6}O_3$ (PZT) films with a Zr/Ti ratio of 40/60, and 5 mol % excess Pb were spin-coated on LNO/Pt/Ti/SiO_2/Si substrates by the sol−gel method. Analytically pure lead acetate trihydrate [$Pb(CH_3COO)_2{\bullet}3H_2O$] (Shanghai Chemical Reagent Co. Ltd.), zirconium nitrate penthydrate [$Zr(NO_3){\bullet}5H_2O$] (Shandong Yantai Keyuan Chemical Reagent Co. Ltd.), and titanium *n*-butoxide [$Ti(OC_4H_9)_4$] (Shanghai Sanaisi Chemical Reagent Co. Ltd.) were used as the starting materials. Lead acetate trihydrate and zirconium nitrate penthydrate are initially dissolved in 2-methoxyethanol and refluxed for 1 h at 100 °C. During the refluxing, an appropriate quantity of acetylacetone is added in the solution to stabilize the solvent system. The associated water is removed during a period of distillation at 125 °C. After cooling to room temperature (RT), the required quantity of titanium *n*-butoxide is added to the solution and mixed in the flask at 80 °C. Then, the solution is refluxed for 1 h and subsequently distilled to remove the byproduct. The solution is testified to be stable and no crystallite forms are observed for several months. The concentration of the final solution can be adjusted to 0.4 M by adding or distilling an appropriate quantity of solvent. The whole process of the preparation of the precursor solution is performed in an ambient atmosphere.[19] Before spin-coated on the substrates, the solution is filtrated with a 0.2 μm syringe filter to avoid particulate contamination. The coating solution for the PZT films is deposited onto Pt/Ti/SiO_2/Si substrates by spin-coating. A layer-by-layer annealing method is carried out in the procedure of heat treatment. The films were deposited by spinning coating at the speed of 4000 rpm for 30 s. Each layer of the films was dried at 180 °C for 3 min, then pyrolyzed at 360 °C for 3 min to remove residual organic compounds, following annealing at 650 °C for 3 min in air by the RTA process. The deposition and annealing-treatment procedures were then repeated many times to obtain a desired film thickness. The detailed growth of the films can be found in ref 19.

XRD and IRSE Measurements. The crystalline structure of the films was analyzed by X-ray diffraction (XRD) using a nickel (Ni) filtered Cu Kα radiation source. In the XRD experiments, a vertical goniometer (model RINT2000) was used, and continuous scanning mode ($2\theta/\theta$) was selected with an interval of 0.02° and scanning rate of 10°/min. The ellipsometric measurements were carried out in the wavelength range of 2.5−12.5 μm (800−4000 cm^{-1}) at RT by a variable-angle IRSE (PhE-104).[25,36] The polarizer and analyzer were synchronously rotated with a speed ratio of 1:1. A liquid nitrogen cooled HgCdTe (MCT) detector was used for SE detection. The system operations, including data acquisition and reduction, preamplifier gain control, incident angle, wavelength setting, and scanning were fully and automatically controlled by the computer. The incident angle can be continuously varied between 20° and 90°. The accuracy was better than 1% for tan Ψ and cos Δ measurements.[25] The incident angles were selected and optimized to 70° and 75° for the multilayer film samples. Note that no mathematical smoothing has been performed for the experimental data.

III. Results and Discussion

Structural Analysis. Figure 1 shows the XRD patterns of the PZT/LNO multilayer films with different associated thickness. It can be shown that the PZT and LNO films are polycrystalline with (100)-preferential orientation and pure perovskite phase. As can be seen, the XRD peaks and/or crystallization of the LNO films strongly depend on the film thickness. However, the XRD patterns of the PZT films do not show the obvious difference with increasing thickness. While the LNO film thickness increases and the PZT film thickness decreases, the diffraction peaks become more intense and sharp. It is noted that there is Pt (200) peak in sample A. The results

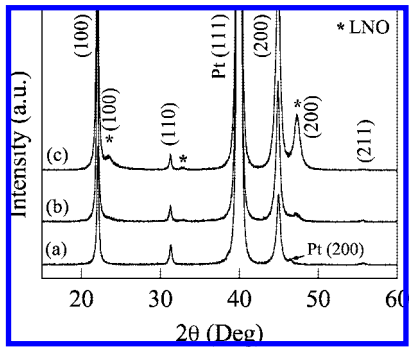

Figure 1. X-ray diffraction patterns of the PZT/LNO multilayer films with different associated thickness (a) 205 nm/29.8 nm, (b) 182 nm/79.2 nm, and (c) 157 nm/146 nm deposited on $Pt/Ti/SiO_2/Si(100)$ substrates.

indicate that the PZT films deposited on the LNO films of the (100)-preferential orientation are also of the highly (100) orientation.

Based on the intensive (100) diffraction peak, the lattice constant a of the PZT films can be calculated with the Lorentz line fitting model, from which the full width at half-maximum (fwhm) and diffraction angle can be readily determined.[37] The a values are 4.019 Å, 4.032 Å, and 4.030 Å for samples A, B, and C, respectively. It suggests that there are different lattice distortions for the PZT films with varied thickness. On the other hand, the grain size r can be estimated from the (100) peak according to the Scherrer equation: $r = K\lambda/\delta \cos\theta$; here, $K \approx 1$ is the shape factor; $\lambda = 1.540$ Å the average wavelength of Cu $K\alpha$ radiation; δ is the fwhm, and θ is the diffraction angle.[38] The average grain sizes were estimated to be about 32 nm, 37 nm, and 40 nm for samples A, B, and C, respectively. It should be emphasized that the crystal strain has been ignored in the estimation of the grain size. It indicates that the film thickness can result in the variations of lattice constant and grain size of the PZT films. Note that the difference of the grain size for the PZT samples is located between 7.5% and 20%. The large variation can obviously contribute to the optical properties.

Theoretical Consideration. In SE, one deals with the measurements of the relative changes in the amplitude and the phase of a linearly polarized monochromatic incident light upon an oblique reflection from the sample surface.[39] The experimental quantities measured by ellipsometry are the angles Ψ and Δ, which are related to the optical and structure properties of the samples and are defined by $\rho = \tilde{r}_p/\tilde{r}_s = \tan\Psi \exp(i\Delta)$. Here $\tilde{r}_p$ and $\tilde{r}_s$ are the complex reflection coefficients of the light polarized parallel and perpendicular to the plane of incidence, respectively. Note that ρ is the function of thickness, photon frequency, and optical constants from the system studied. Although ρ and optical constants may be transformed, there are no corresponding expressions for optical constants, which are distinct for different materials.[40] Therefore, the measured SE spectra from a layer sample may be analyzed using an appropriate fitting model, which is constructed based on the sample layered structure. Generally, the pseudodielectric function $\langle\tilde{\varepsilon}\rangle$ is a useful representation of the ellipsometric data Ψ and Δ by a two-phase (ambient/substrate) model[39]

$$\langle\tilde{\varepsilon}\rangle = \langle\varepsilon_1\rangle + i\langle\varepsilon_2\rangle = \sin^2\phi\left\{1 + \left[\frac{1-\rho}{1+\rho}\right]^2 \tan^2\phi\right\} \quad (1)$$

where ϕ is the incident angle. In this model, unknown parameters, such as thickness and optical constants of each layer, can be designated as fitting variables. As an example, the measured $\langle\varepsilon_1\rangle$ and $\langle\varepsilon_2\rangle$ spectra from samples A and C at

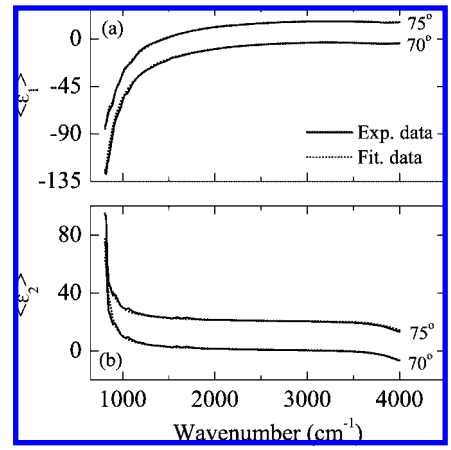

Figure 2. Experimental (solid lines) and fitted data (dotted lines) of the SE parameters (a) $\langle\varepsilon_1\rangle$ and (b) $\langle\varepsilon_2\rangle$ for the PZT/LNO multilayer films with 205 nm/29.8 nm thickness at the incident angles of 70° and 75°. Note that the data at 75° are shifted by 20 in the vertical direction.

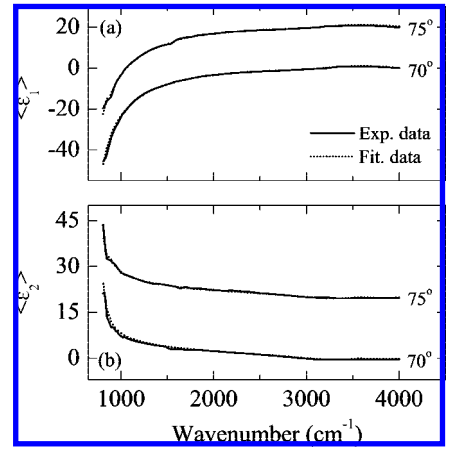

Figure 3. Experimental (solid lines) and fitted data (dotted lines) of the SE parameters (a) $\langle\varepsilon_1\rangle$ and (b) $\langle\varepsilon_2\rangle$ for the PZT/LNO multilayer films with 157 nm/146 nm thickness at the incident angles of 70° and 75°. Note that the data at 75° are shifted by 20 in the vertical direction.

the incident angles of 70° and 75° are shown by the solid lines in Figures 2 and 3, respectively.

The critical step involved in fitting SE data to a given structure model is the proper parametrization of the unknown optical functions. Owing to the complex film stacks, the ellipsometric data were interpreted by the following two independent steps: (1) after the LNO films with different thickness were deposited, the optical constants in the wavenumber region of 800−4000 cm^{-1} and the film thickness can be obtained with a Durde model by the IRSE.[29] The refractive index and extinction coefficient of the LNO films increase with increasing wavelength and indicate that the LNO films are of some metallic characteristics.[29,40] It should be emphasized that the optical constants for LNO materials previously reported have been focused on the visible−ultraviolet photon region, which is far from the present infrared wavelength.[41,42] Therefore, a further comparison with the present data is not possible here. (2) Then, the PZT films were deposited on the LNO films, and infrared optical properties and the thickness were estimated.

In order to extract the optical constants of the PZT films on the LNO bottom electrode, the IRSE spectra were analyzed by a multilayer modeling on the four-phase system (air/PZT/LNO/Pt) as the Pt layers (about 200 nm) were thick enough that the

TABLE 1: Fitted Parameter Values of the Classical Dispersion Model and 90% Confidence Limits in Parentheses for the PZT Films Determined from Figures 2 and 3[a]

parameters	t_{PZT} (nm)	t_{LNO} (nm)	ε_∞	$\sqrt{Nq^2/M^*\varepsilon_0}$ (cm^{-1})	τ ($\times 10^{-10}$ s)
A	205	29.8	5.38	1584	0.48
	(4)	(3.3)	(0.09)	(23)	(0.07)
B	182	79.2	6.50	1786	0.61
	(8)	(8.9)	(0.48)	(95)	(0.06)
C	157	146	7.26	1917	0.78
	(5)	(4)	(0.26)	(45)	(0.06)

[a] Note that t_{PZT} and t_{LNO} are the thickness of the PZT and LNO layers, respectively.

incident infrared light could not propagate through them.[39] In the experimental mid-infrared range, the corresponding photon energy is higher than the phonon frequencies, but much lower than the band gap energy of the PZT films. In the classical theory, for a lower energy electromagnetic field (infrared) propagating in a materials medium, the oscillation equation of motion for the ions in a unit cell is[43]

$$M^*\ddot{x} + \frac{M^*\dot{x}}{\tau} + M^*\omega_0^2 x = qE_0\, e^{i\omega t} \tag{2}$$

where M^* is the reduced mass of cations M_+ and anions M_- in a unit cell ($1/M^* = 1/M_+ + 1/M_-$); q is the ionic average effective charge; ω is the incident infrared frequency; ω_0 is the harmonic oscillation frequency; $qE_0\, e^{i\omega t}$ is the electromagnetic field force acting on atoms, and τ is the energy-independent relaxation time. The last term in eq 2 is the restoring force, which brings ions back to the equilibrium position and is considered to be equal to zero because the optical frequency is high enough that the ion response will lag. Therefore, the solution of eq 2 can be derived as

$$\varepsilon(\omega) = \varepsilon_\infty - \frac{Nq^2}{M^*\varepsilon_0}\frac{\tau^2 - i\tau/\omega}{1+\omega^2\tau^2} \tag{3}$$

where N is the cell number per unit volume and ε_∞ and ε_0 are the high-frequency dielectric constant and the vacuum dielectric constant, respectively.[25,36] Correspondingly, the refractive index n and extinction coefficient κ are decided by the following relationships

$$n = \frac{1}{\sqrt{2}}\sqrt{\sqrt{\varepsilon_1^2+\varepsilon_2^2}+\varepsilon_1} \quad \kappa = \frac{1}{\sqrt{2}}\sqrt{\sqrt{\varepsilon_1^2+\varepsilon_2^2}-\varepsilon_1} \tag{4}$$

A least-squares-fitting procedure employing the modified Levenberg−Marquardt algorithm was used in the fitting. The standard deviations were calculated from the known error bars on the calibration parameters and the fluctuations of the measured data over averaged cycles of the rotating polarizer and analyzer.[22] The unknown optical constants of the PZT films were described using eq 3. The optical constants and film thickness of the LNO films can be obtained in the first step, and the optical constants of Pt were taken from ref 40. We performed the fit to the IRSE data at the incident angles of 70° and 75° simultaneously for the samples with adjustable parameters. The fitted parameter values in eq 3 and the fitted thickness are summarized in Table 1. The fitted $<\varepsilon_1>$ and $<\varepsilon_2>$ spectra for samples A and C are also shown by the dotted lines in Figures 2 and 3, respectively. As we can see, a good agreement is obtained between the experimental and fitted data in the entirely measured energy region. From the pseudodielectric function, it is easy to clarify the spectral influences from Pt and LNO bottom electrodes, which indicates that the main contributions to original IRSE spectra are from the metallic layers due to the high reflection coefficient for infrared light. That is to say, the curves are similar to those of bare Pt substrates.

Parameter Results. From Table 1, the high-frequency dielectric constant of the PZT layers varies approximately from 5.38 to 7.26. Specifically, these data from samples B and C are slightly higher than the reported value of 5.64.[22] Note that the parameter ε_∞ accounts for the so-called high-frequency limit. Therefore, the dielectric function model should be extrapolated to shorter wavelengths than those studied here. However, it is nearly impossible that eq 3 expressing the carrier characteristics can explain the complicated behavior of many high-energy transitions (above the band gap energy) in semiconductor and dielectric materials. Nevertheless, the values are well-located in a reasonable magnitude region, as compared with some typical wide band gap semiconductors and insulators.[25,44]

Note that the parameter $\sqrt{Nq^2/M^*\varepsilon_0}$ is related to the static charges and charge transfer in ABO_3 perovskite materials.[36] It suggests that the charge transfer is not complete for the PZT, which belongs to a mixed ionic−covalent compound. The static charge is an intuitive concept usually based on partitioning the ground-state electronic density into contributions attributed to different atoms. It is noted that the cations M_+ are the sum of atomic weights of Pb, Zr, and Ti, and the anion M_- is the treble atomic weight of O. For the ABO_3 perovskite structures, different approaches have been considered to evaluate the amplitude of the static atomic charges.[45,46] All theoretical calculations and experimental results reveal that charge transfer from Ti (and/or Zr) to O is not complete. Similar results have been found in the $BaTiO_3$ film materials.[25] This may be due to the partial hybridization between Ti (and/or Zr) 3d and O 2p orbital states.[47]

Infrared optical spectra can be used to directly estimate the electrical transport properties of some doped semiconductors and insulators. The relaxation time τ is inversely proportional to the carrier mobility by the average effective mass. Nevertheless, it should be emphasized that the relaxation time at low frequencies is significantly smaller than that in direct-current fields. On the other hand, eq 3 is only an approximation while a more correct approach for the τ should take into account the average carrier-energy distribution at each light frequency.[48] However, the approach becomes very complicated in fitting the IRSE spectra. It can be concluded that the present simple approximation gives reasonable results. The increment of the relaxation time suggests that the mobility decreases. The phenomena can be ascribed to the lattice distortion and grain boundaries from the PZT films with different thickness, some amount of porosity, and amorphous phase as in the following discussion, which can block the carrier movements to some extent. Therefore, it is possible that the IRSE can be applied to characterize the electrical properties for the PZT film materials in connection with the Hall-effect measurements.[49]

Infrared Optical Functions. The optical functions are the basic parameters for IR detector designs. The total absorption of detectors based on ferroelectric materials can be calculated using the obtained dielectric functions.[50] From the fitted results, the associated thickness means that the PZT film thickness increases with decreasing thickness of the LNO films for the PZT/LNO multilayer system. The evaluated optical constants n and κ of the PZT films are shown in Figure 4a,b, respectively. The refractive index of the PZT films decreases as the

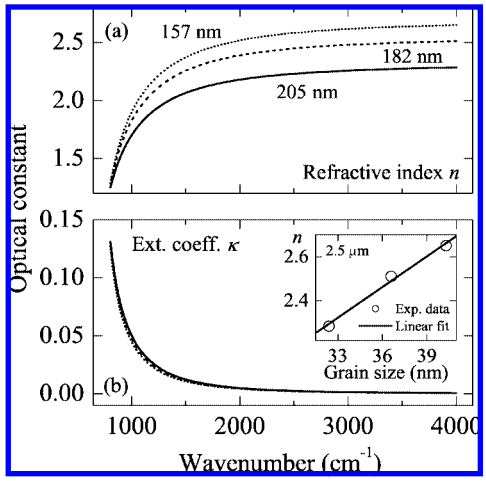

Figure 4. Evolution of the optical constants (a) refractive index and (b) extinction coefficient of the PZT films with different thickness. The inset shows the linear variation of the refractive index with the grain size.

wavenumber decreases, and then approaches unity (normal dispersion). However, the extinction coefficient increases as the wavenumber decreases for all samples. At lower energy side, the n increases and κ decreases with increasing photon energy because of the effects from infrared optical phonon modes, where the abnormal dispersion appears.[25] Moreover, the refractive index of the PZT films increases with decreasing thickness in the entirely measured energy region. The extinction coefficient of the PZT films decreases with decreasing thickness. With the film thickness increasing, the variations of the refractive index and extinction coefficient of the PZT films decrease. In the multilayer film heterostructure, the infrared optical properties are strongly affected not only by the crystallinity of the ferroelectric and bottom electrode films, but also by its particular structure, ferroelectric film thickness, bottom electrode thickness, and so forth.[26,51] It can be believed that the crystallinity and film thickness of the PZT and LNO films induce the changing dependence of the infrared optical properties.

From the XRD patterns of the PZT/LNO multilayer films (see Figure 1), the crystallinity of the PZT films with decreasing thickness is similar. However, the crystallinity of the LNO films is greatly improved with increasing thickness. X-ray diffraction measurements show that the fwhm of the (100) peak in the $PbZr_{0.4}Ti_{0.6}O_3$ layers are 0.278°, 0.246°, and 0.223° for the 205 nm, 182 nm and 157 nm thick films, respectively. The peak position shifts slightly with decreasing thickness, which results in the lattice distortion as in the above discussions. According to the Scherrer equation,[38] the grain size is inversely proportional to the fwhm. So the refractive index of the PZT films linearly increases with increasing grain size, as shown in the inset of Figure 4. On the other hand, the XRD patterns of the PZT films are affected by the orientation of the bottom electrode LNO films. Although the LNO films annealed at 650 °C should have well-defined diffraction peaks, X-ray diffraction spectra taken on the LNO films with the 29.8 nm thickness do not show pronounced peaks because of its small thickness and the absence of texture. However, the XRD patterns of the LNO films with 79.2 nm and 146 nm thickness show the well-defined diffraction peaks. It is possible that the thinner films contain a small fraction of amorphous phase, which cannot be detected by X-ray diffraction. In this case, the variation of the optical constants from the PZT films should be limited by the difference between the crystallinity of the LNO films for the crystalline and amorphous phases, resulting in a large shift of the infrared optical properties.[52,53] Similarly, Petrik et al. reported that the refractive index of the $Ba_{1-x}Sr_xTiO_3$ films decreases with increasing thickness in the visible wavelength range of 350−850 nm.[54] We observed the similar dependence of infrared optical properties from the $Ba_{0.9}Sr_{0.1}TiO_3$ layers on film thickness.[26] Therefore, the thickness of the ferroelectric films and bottom electrodes can greatly affect the infrared optical properties.

To explain this deviation, the assumption that the change in the structure and texture can contribute to the refractive index was presented. Some researchers have explained the shift of the band gap energy in terms of a quantum-size effect in semiconductor and ferroelectric films.[52,55–57] The quantum-size effect results in a dramatic increase in the band gap energy if the crystalline dimensions, namely, the crystalline size, become very small. For the PZT/LNO multilayer films with different associated thickness, the grain size effect can appear not only in the PZT films, but also in the LNO films. The combination of both effects could be responsible for the variations of infrared optical properties for the PZT films. Although there are the sharp features in the interface layer between PZT/LNO and LNO/Pt, the influence of the interface layer maybe contribute to the observed deviation.[58] Because the PZT films are transparent and semitransparent in the measured wavelength region, the reflected light could be interacted with the interface layer. With increasing thickness of the PZT films and decreasing thickness of the LNO films, the effect of the interface layer could be different and induce the variation of the detected light, resulting in the difference of the infrared optical properties. Note that it is not practical to detect the interface layer in the IRSE experiments owing to the long infrared light wavelength, as compared with the interface layer thickness, which is generally about several nanometers.

In addition, the film packing density was increased with increasing thickness. The grain boundaries and morphologies of the PZT and LNO films would depolarize the detected polarizing light. This can also affect the experimental ellipsometric parameters and deteriorate the fitting, which result in the variation of the refractive index for the PZT films. Meanwhile, we do not consider the birefringence of the PZT films during the model fitting in terms of eq 3. The *o*-ray is expected to dominate because it has an entire plane of polarization, whereas the *e*-ray has only one direction of polarization.[36,44,59] It will result in the slight shift of the infrared optical properties because the crystallization of the PZT films strongly depends on the film thickness and orientation of the LNO films. Therefore, it can be concluded that the difference of the infrared optical properties is mainly due to the crystallinity, the grain size effect, and the influence of the interface layer.

The associated thickness of the ferroelectric films and the bottom electrode is one of the important factors in the IRFPA, which can be used to design and estimate the photon response of optoelectronic devices.[50] The absorption coefficient is one of the critical factors for ferroelectric materials in infrared detectors and arrays, which make use of their pyroelectric properties. The absorption coefficient of the PZT films obtained by the formula $\alpha = 4\pi\kappa/\lambda$ is plotted in Figure 5. As can be seen, the absorption coefficient increases rapidly with decreasing wavenumber for all samples. The absorption coefficient of the PZT films linearly increases with increasing thickness in the entirely measured frequency region, as shown in the inset of Figure 5. Meanwhile, the infrared absorption of the PZT films with different thickness is calculated from the derived α and

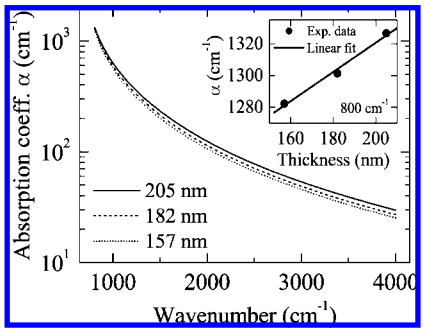

Figure 5. Infrared absorption coefficient of the PZT films with different thickness. The inset shows that it linearly increases with the thickness at the wavenumber of 800 cm^{-1}.

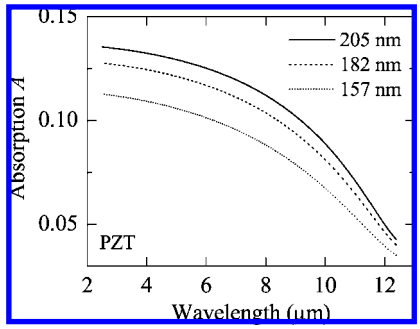

Figure 6. Mid-infrared absorption of the PZT films increases with the thickness. All calculation parameters are from the fitted results in Table 1.

presented in Figure 6. Because the light absorption depends on the film thickness in the opaque range, it increases with the thickness and approaches 10% in the mid-infrared region. Therefore, it will be reasonable to consider the thickness of 205 nm from sample A. The absorption coefficient of the $PbZr_{0.4}Ti_{0.6}O_3$ films is larger than that of the $PbZr_{0.3}Ti_{0.7}O_3$ films and smaller than that of the $PbZr_{0.5}Ti_{0.5}O_3$ films on the similar substrates.[60] It is noted that the thickness of the $PbZr_{0.4}Ti_{0.6}O_3$ films is smaller than those of the compared films. It indicates that the $PbZr_{0.4}Ti_{0.6}O_3$ films may be the most suitable materials for infrared detectors and arrays. Given the infrared semitransparent metal of Ni is used, the Ni/$PbZr_{0.4}Ti_{0.6}O_3$/LNO/Pt heterostructure in this study is a significantly promising resonant microcavity for the pyroelectric IR detectors, as compared with the Ni/$PbZr_{1-x}Ti_xO_3$ ($x = 0.5$ and 0.7)/LNO/Pt structures in the measured wavenumber region.

IV. Conclusion

In summary, the infrared optical properties of the $PbZr_{0.4}Ti_{0.6}O_3$/$LaNiO_3$/Pt/Ti/SiO_2/Si multilayer films with different thickness have been investigated in the photon frequency region of 800−4000 cm^{-1} by fitting the pseudodielectric functions at the incident angles of 70° and 75° with a four-phase layered model. The refractive index of PZT films increases and the extinction coefficient decreases with decreasing thickness. It can be believed that the difference of the infrared optical properties is mainly due to the crystallinity, the grain size effect, and the influence of the interface layer. The absorption coefficient of the $PbZr_{0.4}Ti_{0.6}O_3$ films with smaller thickness is located between those of the $PbZr_{0.3}Ti_{0.7}O_3$ and the $PbZr_{0.5}Ti_{0.5}O_3$ films. It indicates that the $PbZr_{0.4}Ti_{0.6}O_3$ films could be the most suitable materials for IR detectors and arrays. Furthermore, the associated thickness of the ferroelectric films and the bottom electrode is considered to be one of the important factors in IRFPA device design.

Acknowledgment. One of the authors (Z.G.H.) is grateful to Professor Z. M. Huang, X. J. Meng, and G. S. Wang for their technical supports and many fruitful discussions. This work was financially sponsored by Shanghai Pujiang Program (07PJ14034), Major State Basic Research Development Program of China (2007CB924901 and 2006CB921704), Shanghai Municipal Commission of Science and Technology Project (07JC14018 and 07DZ22943), and the Cultivation Fund of the Key Scientific and Technical Innovation Project, MOE of China (No. 704022), and Shanghai Leading Academic Discipline Project (B411).

References and Notes

(1) Sayer, M.; Screenivas, K. *Science* **1990**, *247*, 105.
(2) Trolier-McKinstry, S.; Hu, H.; Krupanidhi, S. B.; Chindaudom, P.; Vedam, K.; Newnham, R. E. *Thin Solid Films* **1993**, *230*, 15.
(3) Lee, J. K.; Kim, T.-Y.; Chung, I.; Desu, S. B. *Appl. Phys. Lett.* **1999**, *75*, 334.
(4) Yan, F.; Wang, Y.; Chan, H. L. W.; Choy, C. L. *Appl. Phys. Lett.* **2003**, *82*, 4325.
(5) Wan, X. M.; Luo, H. S.; Zhao, X. Y.; Wang, D. Y.; Chan, H. L. W.; Choy, C. L. *Appl. Phys. Lett.* **2004**, *85*, 5233.
(6) Fong, D. D.; Stephenson, G. B.; Streiffer, S. K.; Eastman, J. A.; Auciello, O.; Fuoss, P. H.; Thompson, C. *Science* **2004**, *304*, 1650.
(7) Yan, L.; Li, J. F.; Cao, H.; Viehland, D. *Appl. Phys. Lett.* **2006**, *89*, 262905.
(8) Scott, J. F. *Science* **2007**, *315*, 954.
(9) Xiao, B.; Gu, X.; Izyumskaya, N.; Avrutin, V.; Xie, J. Q.; Liu, H. Y.; Morkoç, H. *Appl. Phys. Lett.* **2007**, *91*, 182908.
(10) Scott, J. F.; Araujo, C. A. *Science* **1989**, *246*, 1400.
(11) Xu, Y. H.; Mackenzie, J. D. *Integr. Ferroelectr.* **1992**, *1*, 17.
(12) Hanson, C. M.; Beratan, H. R.; Belcher, J. F.; Udayakumar, K. R.; Soch, K. L. *Proc. SPIE* **1998**, *3379*, 60.
(13) Kohli, M.; Wuethrich, C.; Brooks, K.; Willing, B.; Forster, M.; Muralt, P.; Setter, N.; Ryser, P. *Sensors and Actuators A: Physical* **1997**, *60*, 147.
(14) Willing, B.; Kohli, M.; Muralt, P.; Setter, N.; Oehler, O. *Sensors and Actuators A: Physical* **1998**, *66*, 109.
(15) Leonov, V. N.; Butler, D. P.; Çelik-Butler, Z.; Udayakumar, K. R.; Hanson, C. M.; Beratan, H. R. *Solid-State Electron.* **2001**, *45*, 735.
(16) Lee, H. N.; Hesse, D.; Zakharov, N.; Gösele, U. *Science* **2002**, *296*, 2006.
(17) Watton, R.; Manning, P. *Proc. SPIE* **1998**, *3436*, 541.
(18) Liu, C.; Zou, B. S.; Rondinone, A. J.; Zhang, Z. J. *J. Am. Chem. Soc.* **2001**, *123*, 4344.
(19) Meng, X. J.; Cheng, J. G.; Li, B.; Guo, S. L.; Ye, H. J.; Chu, J. H. *J. Cryst. Growth* **2000**, *208*, 541.
(20) Bao, D. H.; Mizutani, N.; Yao, X.; Zhang, L. Y. *Appl. Phys. Lett.* **2000**, *77*, 1041.
(21) Vurgaftman, I.; Meyer, J. R.; Ram-Mohan, L. R. *J. Appl. Phys.* **2001**, *89*, 5815.
(22) Huang, Z. M.; Meng, X. J.; Yang, P. X.; Zhang, Z. H.; Chu, J. H. *Appl. Phys. Lett.* **2000**, *76*, 3980.
(23) Ariyawansa, G.; Rinzan, M. B. M.; Alevli, M.; Strassburg, M.; Dietz, N.; Perera, A. G. U.; Matsik, S. G.; Asghar, A.; Ferguson, I. T.; Luo, H.; Bezinger, A.; Liu, H. C. *Appl. Phys. Lett.* **2006**, *89*, 091113.
(24) Kang, H. D.; Song, W. H.; Sohn, S. H.; Jin, H. J.; Lee, S. E.; Chung, Y. K. *Appl. Phys. Lett.* **2006**, *88*, 172905.
(25) Hu, Z. G.; Wang, G. S.; Huang, Z. M.; Meng, X. J.; Chu, J. H. *Semicond. Sci. Technol.* **2003**, *18*, 449.
(26) Hu, Z. G.; Wang, G. S.; Huang, Z. M.; Meng, X. J.; Zhao, Q.; Chu, J. H. *Appl. Phys. A: Mater. Sci. Process.* **2004**, *78*, 757.
(27) Kim, S. H.; Woo, H.; Ha, J. J.; Hwang, C. S.; Kim, H. R.; Kingon, A. I. *Appl. Phys. Lett.* **2001**, *78*, 2885.
(28) Angadi, M.; Auciello, O.; Krauss, A. R.; Gundel, H. W. *Appl. Phys. Lett.* **2000**, *77*, 2659.
(29) Hu, Z. G.; Meng, X. J.; Huang, Z. M.; Wang, G. S.; Zhao, Q.; Chu, J. H. *Jpn. J. Appl. Phys.* **2003**, *42*, 7045.
(30) Tompkins, H. G.; Tiwald, T.; Bungay, C.; Hooper, A. E. *J. Phys. Chem. B* **2004**, *108*, 3777.
(31) Hinrichs, K.; Tsankov, D.; Korte, E. H.; Röeler, A.; Sahre, K.; Eichhorn, K. J. *Appl. Spectrosc.* **2002**, *56*, 737.
(32) Hinrichs, K.; Gensch, M.; Esser, N. *Appl. Spectrosc.* **2005**, *59*, 272A.
(33) Hu, Z. G.; Prunici, P.; Patzner, P.; Hess, P. *J. Phys. Chem. B* **2006**, *110*, 14824.
(34) Hu, Z. G.; Hess, P. *J. Vac. Sci. Technol. A* **2007**, *25*, 601.
(35) Meng, X. J.; Cheng, J. G.; Sun, J. L.; Ye, H. J.; Guo, S. L.; Chu, J. H. *J. Cryst. Growth* **2000**, *220*, 100.

(36) Huang, Z. M.; Xue, J. Q.; Ge, Y. J.; Qin, J. H.; Hou, Y.; Chu, J. H.; Zhang, D. H. *Appl. Phys. Lett.* **2006**, *88*, 212902.
(37) Cullety, B. D. *Elements of X-ray Diffraction*; Addison-Wesley: Reading, MA, 1978.
(38) Wilson, A. J. C. *Proc. Phys. Soc. (London)* **1962**, *80*, 286.
(39) Azzam, R. M. A.; Bashara, N. M. *Ellipsometry and Polarized Light*; North-Holland: Amsterdam, The Netherlands, 1977.
(40) Palik, E. D. *Handbook of Optical Constants of Solid*; Academic: New York, 1985.
(41) Mistrik, J.; Yamaguchi, T.; Franta, D.; Ohlidal, I.; Hu, G. J.; Dai, N. *Appl. Surf. Sci.* **2005**, *244*, 431.
(42) Berini, B.; Keller, N.; Dumont, Y.; Popova, E.; Noun, W.; Guyot, M.; Vigneron, J.; Etcheberry, A.; Franco, N.; da Silva, R. M. C. *Phy. Rev. B* **2007**, *76*, 205417.
(43) Chu, J. H.; Sher, A. *Physics and Properties of Narrow Gap Semiconductors*; Springer Science+Business Media, LLC: New York, 2008.
(44) Hu, Z. G.; Weerasekara, A. B.; Dietz, N.; Perera, A. G. U.; Strassburg, M.; Kane, M. H.; Asghar, A.; Ferguson, I. T. *Phy. Rev. B* **2007**, *75*, 205302.
(45) Turik, A. V.; Khasabov, A. G. *Ferroelectrics* **1988**, *83*, 165.
(46) Khatib, D.; Migoni, R.; Kugel, G. E.; Godefroy, L. *J. Phys.: Condens. Matter* **1989**, *1*, 9811.
(47) Cardona, M. *Phys. Rev.* **1965**, *140*, A651.
(48) Songprakob, W.; Zallen, R.; Liu, W. K.; Bacher, K. L. *Phys. Rev. B* **2000**, *62*, 4501.
(49) Kasic, A.; Schubert, M.; Einfeldt, S.; Hommel, D.; Tiwald, T. E. *Phys. Rev. B* **2000**, *62*, 7365.
(50) Bauer, S.; Bauer-Gogonea, S.; Ploss, B. *Appl. Phys. B: Lasers and Optics* **1992**, *54*, 544.
(51) Liu, W. G.; Ko, J. S.; Zhu, W. G. *Infrared Phys. Technol.* **1999**, *41*, 169.
(52) Bao, D. H.; Yao, X.; Wakiya, N.; Shinozaki, K.; Mizutani, N. *Appl. Phys. Lett.* **2001**, *79*, 3767.
(53) Majumder, S. B.; Jain, M.; Katiyar, R. S. *Thin Solid Films* **2002**, *402*, 90.
(54) Petrik, P.; Khanh, N. Q.; Horvath, Z. E.; Zolnai, Z.; Lohner, I.; Fried, M.; Gyulai, J.; Schmidt, C.; Schneider, C.; Ryssel, H. *J. Non-Cryst. Solids* **2002**, *303*, 179.
(55) Alivisatos, A. P. *Science* **1996**, *271*, 933.
(56) Kosacki, I.; Petrovsky, V.; Anderson, H. U. *Appl. Phys. Lett.* **1999**, *74*, 341.
(57) Chen, C. W.; Chen, K. H.; Shen, C. H.; Ganguly, A.; Chen, L. C. *Appl. Phys. Lett.* **2006**, *88*, 241905.
(58) Hu, Z. G.; Huang, Z. M.; Wu, Y. N.; Wang, G. S.; Meng, X. J.; Shi, F. W.; Chu, J. H. *J. Vac. Sci. Technol. A* **2004**, *22*, 1152.
(59) Sanjurjo, J. A.; Porto, S. P. S.; Silberman, E. *Solid State Commun.* **1979**, *30*, 55.
(60) Yu, J.; Huang, Z. M.; Meng, X. J.; Sun, J. L.; Chu, J. H.; Tang, D. Y. *Appl. Phys. Lett.* **2001**, *78*, 793.

JP801566B